International Journal of Pharmaceutics: X 7 (2024) 100240

Contents lists available at ScienceDirect

International Journal of Pharmaceutics: X

journal homepage: www.sciencedirect.com/journal/international-journal-of-pharmaceutics-x

Spanlastic-laden nanogel as a plausible platform for dermal delivery of bimatoprost with superior cutaneous deposition and hair regrowth efficiency in androgenic alopecia

Bjad K. Almutairy [a], El-Sayed Khafagy [a,b,*], Mohammed F. Aldawsari [a], Abdullah Alshetaili [a], Hadil Faris Alotaibi [c], Amr Selim Abu Lila [d,e]

[a] Department of Pharmaceutics, College of Pharmacy, Prince Sattam Bin Abdulaziz University, Al-kharj 11942, Saudi Arabia
[b] Department of Pharmaceutics and Industrial Pharmacy, Faculty of Pharmacy, Suez Canal University, Ismailia 41522, Egypt
[c] Department of Pharmaceutical Sciences, College of Pharmacy, Princess Nourah Bint AbdulRahman University, P.O. Box 84428, Riyadh 11671, Saudi Arabia
[d] Department of Pharmaceutics and Industrial Pharmacy, Faculty of Pharmacy, Zagazig University, Zagazig 44519, Egypt
[e] Department of Pharmaceutics, College of Pharmacy, University of Hail, Hail 81442, Saudi Arabia

ARTICLE INFO

Keywords:
Androgenic alopecia
Bimatoprost
Dermal delivery
Skin deposition
Spanlastics

ABSTRACT

Bimatoprost (BIM) is a prostaglandin F2α analogs originally approved for the treatment of glaucoma and ocular hypertension. Recent studies have highlighted its potential to boost hair growth. The objective of this investigation is to challenge the potential of spanlastics (SLs) as a surfactant-based vesicular system for promoting the cutaneous delivery of BIM for the management of alopecia. BIM-loaded spanlastics (BIM-SLs), composed of Span as the main vesicle component and Tween as the edge activator, were fabricated by ethanol injection method. The formulated BIM-SLs were optimized by 2^3 full factorial design. The optimized formula (F1) was characterized for entrapment efficiency, surface charge, vesicle size, and drug release after 12 h (Q_{12h}). The optimized formula (F1) exhibited high drug entrapment efficiency (83.1 ± 2.1%), appropriate zeta potential (−19.9 ± 2.1 mV), Q_{12h} of 71.3 ± 5.3%, and a vesicle size of 364.2 ± 15.8 nm, which favored their cutaneous accumulation. In addition, *ex-vivo* skin deposition studies revealed that entrapping BIM within spanlastic-based nanogel (BIM-SLG) augmented the dermal deposition of BIM, compared to naïve BIM gel. Furthermore, *in vivo* studies verified the efficacy of spanlastic vesicles to boost the cutaneous accumulation of BIM compared to naive BIM gel; the $AUC_{0\text{-}12h}$ of BIM-SLG was 888.05 ± 72.31 μg/mL.h, which was twice as high as that of naïve BIM gel ($AUC_{0\text{-}12h}$ 382.86 ± 41.12 μg/mL.h). Intriguingly, BIM-SLG outperforms both naïve BIM gel and commercial minoxidil formulations in stimulating hair regrowth in an androgenetic alopecia mouse model. Collectively, spanlastic vesicles might be a potential platform for promoting the dermal delivery of BIM in managing alopecia.

1. Introduction

Alopecia is defined as abnormal hair loss that is usually accompanied by alterations in the normal hair development cycle such as diminished anagen phase and extended catagen/telogen phases (Qi and Garza, 2014). Aging, heredity, hormonal imbalances, dietary deficiencies, and autoimmune illnesses all contribute to changes in the hair cycle (Gokce et al., 2022). Even though alopecia does not cause serious physical discomfort, it has considerable negative psychological and social consequences. As a result, treating alopecia is essential to support patients' well-being.

The current pharmacologic therapies for alopecia target alleviating dihydrotestosterone and/or activating hair follicles *via* the use of oral 5-α reductase antagonists such as finasteride or topical vasodilators such as minoxidil (Adil and Godwin, 2017; Suchonwanit et al., 2019). However, these treatment options elicit undesirable adverse effects; finasteride remarkably decreases dihydrotestosterone serum concentrations, triggering sexual side effects, whilst topical minoxidil commonly provokes pruritus and irritating contact dermatitis (Albash et al., 2022). These elicited adverse effects exert a negative impact on patients' compliance and consequently compromise patients' adherence to therapy.

* Corresponding author at: Department of Pharmaceutics, College of Pharmacy, Prince Sattam Bin Abdulaziz University, Al-kharj 11942, Saudi Arabia.
E-mail addresses: b.almutairy@psau.edu.sa (B.K. Almutairy), e.khafagy@psau.edu.sa (E.-S. Khafagy), moh.aldawsari@psau.edu.sa (M.F. Aldawsari), a.alshetaili@psau.edu.sa (A. Alshetaili), hfalotaibi@pnu.edu.sa (H.F. Alotaibi), a.abulila@uoh.edu.sa (A.S.A. Lila).

https://doi.org/10.1016/j.ijpx.2024.100240
Received 22 February 2024; Received in revised form 19 March 2024; Accepted 24 March 2024
Available online 26 March 2024

Instead, drug repurposing has emerged as a promising approach to find out new alopecia therapies based on repurposing currently approved drugs, which were incidentally observed to exert positive effects on hair regrowth. Among them, prostaglandin (PG) analogs have been recently acknowledged for their ability to promote hair growth (Chen et al., 2022; Jiang et al., 2023). Generally, hair growth is stimulated by PGE2 and PGF2α, while it is inhibited by PGD2 (Heilmann et al., 2013). Bimatoprost (BIM) is a prostaglandin F2α analogs (PGAs) originally approved for treating glaucoma and ocular hypertension (Satyanarayana et al., 2023). In addition, BIM is the only approved treatment for hypotrichosis and alopecia of the eyelashes (Barrón-Hernández and Tosti, 2017). Bimatoprost is reported to boost hair growth by accelerating the transition from the telogen to anagen phase, and increasing the duration of the anagen phase, resulting in increased hair length (Cohen, 2010; Law, 2010). Nevertheless, up to date, only scarce studies had explored the potential of topical BIM for treating androgenic alopecia. Subedi et al. (Subedi et al., 2022) have emphasized the superior efficacy of 5% topical BIM to enhance hair regrowth in androgenic alopecia mouse model, compared to 5% topical minoxidil formulation, with minimum side effects. In another randomized clinical trials, topical application of 0.3% BIM solution for 12 successive weeks resulted in a remarkable increment in terminal hair diameter and count, which was comparable to minoxidil 5% solution (Tabri et al., 2018). Collectively, these studies underscored the efficacy of BIM in activating hair growth. Nevertheless, these reports did not address how to increase the skin delivery of this drug.

The main obstacle for cutaneous drug delivery is the prominent barrier of the outermost skin layer (stratum corneum), which restricts drug permeation and makes it difficult to achieve adequate therapeutic doses. A wide range of approaches have been adopted to overcome skin limited permeability and to attain adequate drug levels in the hair follicle (Sallam et al., 2021a). Nano-vesicular systems such as liposomes and niosomes have been widely employed in dermal drug delivery (Abu-Huwaij et al., 2023; Pierre and dos Santos Miranda Costa, 2011; Schreier and Bouwstra, 1994). They offer the advantages of delivering hydrophilic and hydrophobic drugs to target site, controlling/sustaining drug release, and most importantly, overcoming skin barrier (Abu-Huwaij et al., 2023; Li et al., 2022). Recently, spanlastics have attracted a lot of interest as a plausible drug delivery system with more flexibility and penetrability through various skin layers than traditional vesicles (liposomes and niosomes) (Ansari et al., 2022). Spanlastics are elastic surfactant-based nanovesicles composed mostly of non-ionic surfactants and edge activators (EA) (Almutairy et al., 2023). The inclusion of EA to vesicles bestows spanlastics with a great elasticity, which significantly augment spanlastics payload permeation across biological membranes (Farghaly et al., 2017). In addition, spanlastics are more physically and chemically stable than phospholipid-based counterparts (Al-mahallawi et al., 2017). Furthermore, these deformable spanlastics outperform niosomes in terms of not only overcoming the stratum corneum barrier but penetrating various skin layers by squeezing through skin channels and pores as well (Al-mahallawi et al., 2017; Sallam et al., 2021b). Consequently, spanlastics could efficiently improve the dermal delivery of entrapped drugs and prolong their residence within different skin layers.

The aim of this investigation, therefore, was to formulate topical bimatoprost-loaded spanlastics (BIM-SLs) for facilitating dermal delivery and augmenting BIM skin bioavailability. BIM-SLs were fabricated by ethanol injection method and the optimized formula was characterized. In addition, the *ex-vivo* skin permeability, *in vivo* dermato-kinetic profile and *in vivo* efficacy in an androgenic alopecia mouse model were studied.

2. Materials and methods

2.1. Materials

Bimatoprost (BIM), Span 60, Span 80, Tween 20 and Tween 80 were procured from Sigma-Aldrich (St. Louis, MO, USA). HPMC K4M was provided by Loba-Chemie, Mumbai, India. Other chemicals and solvents were of analytical grade.

2.2. Preparation of bimatoprost-loaded spanlastics (BIM-SLs)

The ethanol injection method was utilized to fabricate bimatoprost-loaded spanlastic (BIM-SLs) vesicles. Briefly, 5 mg of BIM and definite weights of non-ionic surfactants (Span 60 or Span 80) were dissolved in 5 mL ethanol and slowly injected into an aqueous solution (70 °C) of different grades of Tweens (Tween 20 or Tween 80) as an edge activator (EA) under magnetic stirring. The study examined various ratios of Span to EA, which were 9:1 (180 mg of Span: 20 mg EA), and 8:2 (160 mg of Span: 40 mg EA), respectively. The resulting dispersion was subjected to bath-sonication for 5 min to reduce vesicle size. The formed BIM-SLs vesicles were then stored at 4 °C for further analysis (Sallam et al., 2021b).

2.3. Experimental design

Three factor, two levels (2^3) factorial design using Design-Expert® software was utilized to prepare and optimize BIM-SLs. The impact of three independent formulation variables, namely, type of vesicle forming non-ionic surfactant (A), type of EA (B), and ratio of non-ionic surfactant to EA (C), on three formulation characteristics; vesicle size (R_1), percentage entrapment efficiency (R_2), and % BIM released after 12 h (Q_{12h}) (R_3) was explored (Table 1). A Total of eight formulations were developed based on 2^3 factorial design as tabulated in Table 2. The obtained data were statistically analyzed using analysis of variance (ANOVA) to assess whether or not the independent variables had significant influence on tested responses. Furthermore, the fitness of the selected model to the experimental findings was judged by comparing the values of the predicted R^2 with adjusted R^2.

2.4. Characterization of BIM-SLs

2.4.1. Determination of vesicle size and zeta potential

BIM-SLs vesicle size and surface charge were estimated at 25 °C using Nano-ZS 90 Zetasizer (Malvern instruments Ltd., UK), following appropriate dilution with deionized water (1:100). All measurements were conducted in triplicates (Al Hagbani et al., 2022).

2.4.2. Determination of entrapment efficiency

The entrapment efficiency (EE%) of BIM-SLs was determined indi-

Table 1
2^3 factorial design for BIM-loaded spanlastics.

Independent variables	Levels	
	Low (−1)	High (+ 1)
A: Type of Span	Span 60	Span 80
B: Type of EA	Tween 20	Tween 80
C: Ratio of Span:EA	9:1	8:2

Responses	Constrains
R_1: Vesicle size (nm)	In range*
R_2: entrapment efficiency (%)	Maximize
R_3: Q_{12h} (%)	Minimize

* In range reveals that vesicle size lies in the range of $200 \leq R_1 \leq 400$ nm.

Table 2
Composition of BIM-SLs and their obtained responses.

Formula	Formulation parameters			Formulation Responses		
	A	B	C	R_1 (nm)	R_2 (%)	R_3 (%)
F1	Span 60	Tween 80	9:1	364.2 ± 15.8	83.1 ± 2.1	71.3 ± 5.3
F2	Span 80	Tween 20	8:2	322.2 ± 16.1	54.3 ± 0.9	89.3 ± 5.7
F3	Span 80	Tween 80	8:2	256.8 ± 14.3	61.9 ± 1.1	84.6 ± 6.2
F4	Span 80	Tween 20	9:1	462.3 ± 11.3	59.8 ± 1.3	85.7 ± 4.9
F5	Span 60	Tween 80	8:2	240.7 ± 12.1	79.6 ± 1.6	77.1 ± 3.7
F6	Span 80	Tween 80	9:1	391.6 ± 17.6	66.1 ± 1.0	82.4 ± 4.8
F7	Span 60	Tween 20	8:2	276.1 ± 9.9	67.3 ± 0.9	81.1 ± 3.4
F8	Span 60	Tween 20	9:1	431.7 ± 19.4	73.1 ± 0.8	78.6 ± 3.1

A: type of span; B: type of EA; C: Span:EA ratio R_1: vesicle size R_2: %EE; and R_3: Q_{12h} (%). The data are the mean ± SD; $n = 3$.

rectly using ultracentrifugation technique. Briefly, 1 mL of BIM-SLs dispersion was subjected to centrifugation at 4 °C for 60 min at 15,000 rpm to separate the un-encapsulated drug. The concentration of free BIM in the supernatant was analyzed spectrophotometrically at 294 nm. The EE% was then calculated using the following equation:

$$\%EE = \frac{(Total\ initial\ amount\ of\ BIM – amount\ of\ free\ BIM)}{Total\ initial\ amount\ of\ BIM}\ x\ 100$$

2.4.3. Differential scanning calorimetry (DSC)

A Shimadzu DSC 60 (Tokyo, Japan) was utilized to screen the thermal behavior of different spanlastic components. In brief, 2 mg samples of pure BIM, Span 60, Tween 80 and optimized BIM-SLs were filled in typical aluminum pans and then heated from 0 to 300 °C with a scanning rate of 10 °Cmin^{-1} under a nitrogen purge (Al Saqr et al., 2021).

2.4.4. Determination of BIM-SLs elasticity

The elasticity of BIM-SLs dispersion was assessed by extrusion method. Briefly, the optimized BIM-SLs formula was extruded through a membrane filter (polycarbonate, 0.1 μm pore size) at constant pressure of 2.5 bar (Badria and Mazyed, 2020). Then, the size of the extruded vesicles was measured and compared with that prior to extrusion. Finally, vesicle elasticity was determined in terms of deformability index (DI) using the following formula:

$$DI = J\ (r_v/r_p) \quad (2)$$

where J is the amount of sample extruded, r_v is the vesicle size after extrusion, while r_p is the pore size of extruding membrane in nm.

2.5. In vitro release study of BIM-SLs

A modified Franz diffusion cell was utilized to explore the *in vitro* release profile of BIM-loaded SLs. Initially, cellulose membrane (MW cut-off 12,000–14,000 KDa) was hydrated overnight using a phosphate buffer solution (pH 7.4). The cellulose membrane was then fitted between the receptor and donor cells of Franz diffusion cell. A definite volume of optimized BIM-SLs (equivalent to 3 mg BIM) was placed in the donor compartment and the receptor compartment was filled with 100 mL of phosphate buffer solution (pH 7.4) stirred at 100 rpm at 37 ± 0.5 °C. At pre-determined time points (0.5, 1, 2, 4, 8, and 12 h), aliquot samples (2 mL) were withdrawn, and the concentration of BIM was quantified spectrophotometrically at 294 nm.

2.6. Physical stability of BIM-SLs

To address the impact of storage on the physical stability of optimized BIM-SLs (F1), BIM-SLs was placed in a securely closed glass vial and stored at 4 °C for 90 days. The optimized BIM-SLs were tested with respect to their vesicle size and EE% at various time points and compared with those of fresh formulation.

2.7. Preparation of BIM-loaded spanlastic gel (BIM-SLG)

In order to ease the application of optimized BIM-SLs and to prolong formulation contact time of formulation with the scalp, Optimized BIM-SLs vesicles were incorporated in hydroxypropyl methylcellulose (HPMC)-based gel system. Briefly, an accurately weighed amount of 2% HPMC K4M (0.2 g) were sprinkled into distilled water (10 mL) with constant stirring until the attainment of a homogenous gel base. BIM-loaded spanlastic gel (BIM-SLG) was obtained by dispersing a definite weight of optimized BIM-SLs into the gel base, yielding a BIM-SLG formula with a total BIM concentration of 0.3% *w*/w. For the preparation of BIM gel, pure BIM was incorporated into HPMC gel base instead of optimized BIM-SLs formula.

2.8. Characterization of BIM-loaded spanlastic gel (BIM-SLG)

The organoleptic properties (color, homogeneity and clarity) of the formulated BIM-SLG were assessed by visual inspection. Drug content was quantified spectrophotometrically at 294 nm. The pH of gel formulations was recorded by a glass electrode-based pH-meter. Viscosity measurements were conducted at a rotational speed of 5 rpm using Brookfield viscometer (model-LV, Brookfield, Middleboro, MA, USA). The gel's spreadability was assessed using the glass slide method (Nurman et al., 2019).

2.9. Skin Permeation study

The *ex vivo* skin permeation profile of BIM-loaded spanlastic gel (BIM-SLG) through rat abdominal skin was investigated utilizing Franz diffusion cell with a diffusion surface area of 1.76 cm^2. *Ex vivo* tissues, skin, were obtained under veterinary supervision from male albino rats and according to the Ethics Committee of Animals Experimentation at Prince Sattam Bin Abdulaziz University, Al-Kharj, KSA (approval number: 048/2022). The receptor media consisted of 100 mL of phosphate buffer solution (pH 5.5) stirred at 50 rpm at 35 ± 1 °C. The rat skin was mounted with the stratum corneum facing the donor compartment. A specified weight of tested formulations (either the optimized BIM-SLG or pure BIM gel, corresponding to 3 mg BIM, was put into the donor compartment. 2 mL samples were withdrawn at various time intervals and replenished with equal volume of release buffer. The cumulative amount of BIM permeated per unit area of skin was graphed against time. Permeation parameters including steady-state flux (J_{ss}; μg/cm^2.h), cumulative amount permeated per unit area after 12 h (Q_{12h}), cumulative amount deposited per unit area after 12 h (Dep_{12h}), and the local accumulation efficiency index (LAEI); computed as the ratio of BIM deposited within the skin to that permeated *via* the skin, were calculated (Albash et al., 2021).

Finally, skin samples were collected, cleaned with phosphate buffer, and then homogenized with methanol to extract BIM that remained in the skin. Skin homogenate was then centrifuged at 10000 rpm for 15 min and BIM content in the supernatant was quantified by HPLC analysis as previously described (Zezula et al., 2019). Briefly, HPLC system (Shimadzu, Kyoto, Japan) fitted with a Hypersil® C-18 column (1.5 cm × 4.6 mm, 5 μm) was employed. A 20 μL samples was eluted using a mobile phase consisting of 0.01% orthophosphoric acid:acetonitrile (80:20 *v*/v), adjusted to pH 2.8. A UV–Visible detector operating at 205 nm was used for detection.

2.10. In vivo studies

2.10.1. Animals

6-week-old male C57BL/6 mice (20 g–25 g) and male Albino rats (200–250 g) were used for *in vivo* experiments. The animals were kept under standard laboratory conditions of temperature, humidity, and 12-h day–night cycle with easy access to water and food. All experimental procedures were revised and approved by Ethical Committee, Prince Sattam Bin Abdulaziz University, Al-Kharj, KSA (approval number: 048/2022), and *in vivo* studies were performed in alignment with ARRIVE guidelines.

2.10.2. In vivo skin deposition study

Male albino rats were randomly categorized into two groups of 18 rats each. The first group was topically treated with 0.3% BIM gel, while the second group was topically treated with 0.3% BIM-loaded spanlastic gel (BIM-SLG) (Subedi et al., 2022). At specified time intervals post gel application, three rats from each group were euthanized, skin was excised, cut into pieces and vortexed with methanol for 30 min to extract BIM. BIM concentration was then quantified by HPLC as aforementioned. Finally, dermato-kinetic parameters such as T_{max}, C_{max} and $AUC_{0\text{-}12h}$ were calculated using a PKSolver 2.0 software.

2.10.3. In vivo hair regrowth efficacy of BIM formulations

The hair regrowth efficiency of different BIM formulations was assessed using an androgenetic alopecia mouse model (Fu et al., 2021). Briefly, 6-week-old male C57BL/6 mice (20 g–25 g) were treated topically with dihydrotestosterone (0.5 mg/kg) once daily for five consecutive days to induce androgenic alopecia, and then dorsal hair was shaved using animal clippers. Animals that show skin lesions or skin injuries were excluded from this study. The animals were then randomly divided into 4 groups of 6 mice each. Group I was treated with blank spanlastic gel and served as control. Group II was treated with plain BIM gel (0.3% *w*/w) (Subedi et al., 2022). Group III was treated with optimized BIM-loaded spanlastic gel (BIM-SLG; 0.3% w/w). Group IV was treated with commercial minoxidil topical solution (5%) and served as a positive control. All treatments were applied topically once daily for 14 consecutive days. An additional group of 6 mice were shaved with clippers and served as normal controls. At definite time intervals (0, 7, 10, and 14 days) post-treatment, hair regrowth was examined in terms of length of hair follicle using a Vernier digital caliper for 20 hairs per mice (Zhang et al., 2021). In addition, at day 14 post-treatment, the regrown hair in the treatment area was cut and weighed by an analytical balance (Orasan et al., 2016). Statistical analysis was performed with a one-way analysis of variance (ANOVA) followed by Tukey *post hoc* test using the Prism 8 software (GraphPad Software, San Diego, CA, USA). Results are presented as means ± standard deviations, and statistical significance was accepted for p values <0.05.

3. Results and discussion

3.1. Analysis of factorial design

2^3 full factorial design was adopted to scrutinize the impact of various formulation variables on the properties of formulated BIM-loaded spanlastics (BIM-SLs). Eight experimental runs (F1-F8) were fabricated at three different formulation variables; type of surfactant (span) (A), type of EA (B), and ratio of Span:EA (C) and were examined at two levels (Table 1). Table 2 illustrates the measured responses for all BIM-SLs formulations. Statistical analysis of model output data verified the good fit of all the tested responses to the linear model since the predicted R^2 values were in reasonable agreement with the Adjusted R^2 *i.e.* the difference is <0.2 (Table 3).

In addition, regression equations were created to depict the relationship between specified independent variables and tested formulation attributes, as well as to determine the relative effect of each variable on product characteristics.

$$\text{Vesicle size } (R_1) = +343.2 + 15.03\ A - 29.87\ B + 69.25C.$$

$$\text{EE } (\%)\ (R_2) = 68.15 - 7.62\ A + 4.53\ B + 2.37C.$$

$$Q_{12h}\ (\%)\ (R_3) = 81.26 + 4.24\ A - 2.41\ B - 1.76C.$$

The positive sign indicates a synergistic impact on the tested response, while a negative sign implies an antagonistic effect on the tested response.

Table 3
Output data of the 2^3 factorial design of BIM-loaded spanlastics.

Responses	R^2	Adjusted R^2	Predicted R^2	Adequate precision
Vesicle size (R_1)	0.9638	0.9366	0.8551	16.321
EE (%) (R_2)	0.9845	0.9729	0.9382	25.255
Q_{12h} (%) (R_3)	0.9757	0.9575	0.9028	20.5646

3.1.1. Influence of formulation variables on BIM-SLs vesicle size (R_1)

The vesicle size of all fabricated BIM-SLs varied from 240.7 ± 12.1 nm to 462.3 ± 11.3 nm (Table 2). Statistical analysis demonstrated that all tested formulation variables significantly affected the vesicle size of prepared BIM-SLs (Table 4).

Regarding the type of non-ionic surfactant (A), it was evident that the type of non-ionic surfactant had a significant impact on the vesicle size of formulated BIM-SLs. Spanlastic vesicles prepared with span 60 exerted smaller vesicle size than those prepared with span 80 (Fig. 1). At fixed ratio of Span:EA and by using the same EA, F7 prepared with span 60 exerted a vesicle size of 276.1 ± 99 nm, which was significantly smaller than that prepared with span 80 (F2; 322.2 ± 16.1 nm). This might be accredited to the presence of unsaturation in Span 80, which would favor the formation of enlarged bilayered-nano-vesicles (Akbari et al., 2015). Similar findings were testified by Mazyed et al. who emphasized the impact of Span type on the vesicle size of epigallocatechin gallate-loaded spanlastics (Mazyed et al., 2021).

Similarly, increasing Span:EA ratio from 8:2 to 9:1 exerted a positive on BIM-SLs vesicle size. BIM-SLs prepared at Span:EA ratio of 9:1 (F4) showed a vesicle size of 462.3 ± 11.3 nm, which was remarkably larger than that of BIM-SLs prepared at Span:EA ratio of 8:2 (F2; 322.2 ± 16.1 nm). This might be explained by the fact that increasing EA amount, as observed at Span:EA ratio of 8:2, would, on the one hand, decrease the interfacial tension, resulting in the formation of small vesicles (Badria and Mazyed, 2020), and on the other hand, would promote the development of mixed micelles with smaller sizes rather than bilayered vesicles (Basha et al., 2013).

By contrary, EA type exerted a negative effect on BIM-SLs vesicle size. Spanlastic vesicles prepared with Tween 20 as an EA exerted a larger size than those prepared with Tween 80. The vesicle size of BIM-

Table 4
ANOVA for the 2^3 factorial design of BIM-SLs.

Independent variable	Source	Sum of Squar	Df	Mean Square	F-Value	*p*-Value
Vesicle size (R_1)	Model	45,877.01	3	15,292.34	35.49	0.0024
	A	3415.51	1	3415.51	7.93	0.0481
	B	10,089.10	1	10,089.10	23.41	0.0084
	C	32,372.40	1	32,372.40	75.12	0.0010
%EE (R_2)	Model	674.05	3	224.68	84.91	0.0004
	A	465.12	1	465.12	175.77	0.0002
	B	163.80	1	163.80	61.90	0.0014
	C	45.12	1	45.12	17.05	0.0145
Q_{12h} (R_3)	Model	215.06	3	71.69	53.55	0.0011
	A	143.65	1	143.65	107.30	0.0005
	B	46.56	1	46.56	34.78	0.0041
	C	24.85	1	24.85	18.56	0.0126

Values of $p < 0.05$ indicate the significance of model terms.

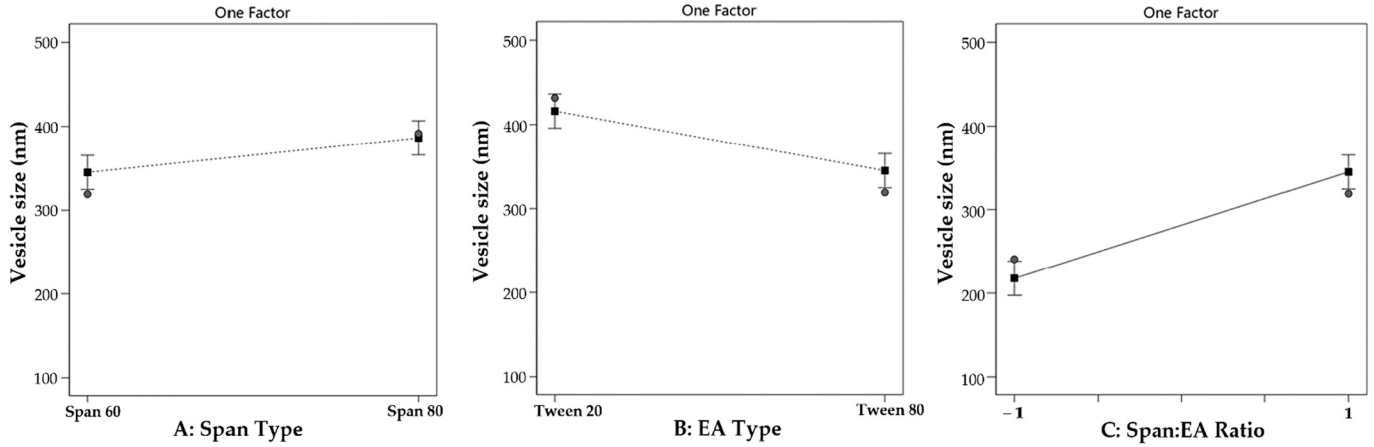

Fig. 1. The impact of various independent variables; Type of Span (A), type of EA (B), and Span:EA ratio (C) on Vesicle size.

SLs prepared with Tween 80 (F3) was 256.8 ± 14.3 nm, which was smaller than that of F2 (322.2 ± 16.1 nm), fabricated with Tween 20. The smaller vesicle size of BIM-SLs prepared with Tween 80 (HLB 14.9) compared to those prepared with Tween 20 (HLB 16.7) might be accounted for the lower hydrophilicity; lower HLB, of Tween 80, which would result in a decrease in the surface energy and the formation of smaller nanovesicles (ElMeshad and Mohsen, 2016; Yusuf et al., 2014).

3.1.2. *Influence of formulation variables on percentage entrapment efficiency (EE% (R_2))*

The ability of nano-vesicular systems to efficiently entrap the bioactive drug is considered a key parameter that dictates the efficiency of dermal delivery. As tabulated in Table 2, the EE% of various BIM-SLs fluctuated from 54.3 ± 0.9% to 83.1 ± 2.1%. Fig. 2 illustrates how different formulation variables affect the %EE of BIM-SLs. Statistical analysis results (Table 4) indicate that all the tested variables had a substantial influence on the %EE of the spanlastic formulations. With respect to the type of non-ionic surfactant (A), it was clear that Span 60-based spanlastic vesicles had considerably higher %EE than Span 80-based vesicles. At fixed Span:EA ratio and upon using the same EA, BIM SLs prepared with Span 60 (F5) had %EE of 79.6 ± 1.6%, which was significantly higher than that of F3 (%EE 61.9 ± 1.1%) prepared with Span 80. This might be attributed to the higher phase transition temperature (T_c = 53 °C) of Span 60, compared to that of Span 80 (T_c − 12 °C), which result in reduced drug leakage from Span 60-based SLs (Ruckmani and Sankar, 2010).

Additionally, EA type (B) had a significant influence on %EE ($p < 0.01$). spanlastic vesicles prepared with Tween 20 exerted a lower %EE than those fabricated with Tween 80. At the same Span:EA ratio and using Span 80 as the main vesicle component, BIM-SLs prepared with Tween 20 (F2) showed a percentage entrapment efficiency (%EE) of 54.3 ± 0.9, which was considerably lower than that of F3 (%EE 61.9 ± 1.1%), fabricated with Tween 80. This could be ascribed to the lower HLB value of Tween 80 (HLB 14.9) compared to Tween 20 (HLB 16.7); where lower HLB value designates higher hydrophobicity, and increased membrane integrity, which would augment BIM entrapment within the fabricated vesicles (Guinedi et al., 2005; Moawad et al., 2017).

Finally, Span:EA ratio (C) exerted a positive effect on %EE ($p < 0.05$) on BIM entrapment within spanlastic vesicles. Spanlastic vesicles prepared at Span:EA ratio of 9:1, using the same type of Span and Tween, showed significantly higher %EE than those prepared at Span:EA ratio of 8:2. Increasing EA amount, as observed at Span:EA ratio of 8:2, would result in increased spanlastic membrane fluidity, which would permit the leakage of the entrapped drug and consequently resulted in reduced %EE (Duangjit et al., 2011). Similar results were reported by Moawad et al. who point out the negative effect of increasing EA amount on the encapsulation of the antispasmodic drug, tizanidine HCl, within nano-transferosome vesicles (Moawad et al., 2017).

3.1.3. *Influence of formulation variables on Q_{12h} from BIM-SLs (R_3)*

The *in vitro* release profiles of BIM-SLs, as well as free drug, are represented in Fig. 3. As depicted in Fig. 3, all BIM-SLs formulations displayed a sustained release profile that fluctuated from 71.3 ± 5.3% (F1) to 89.3 ± 5.7% (F2) after 12 h. These results underscored the efficacy of spanlastic vesicles to act as reservoirs for BIM for dermal delivery. By contrary, free BIM showed a higher drug release of >90% after 4 h.

The effect of different formulation variables on Q_{12h} of BIM-SLs is

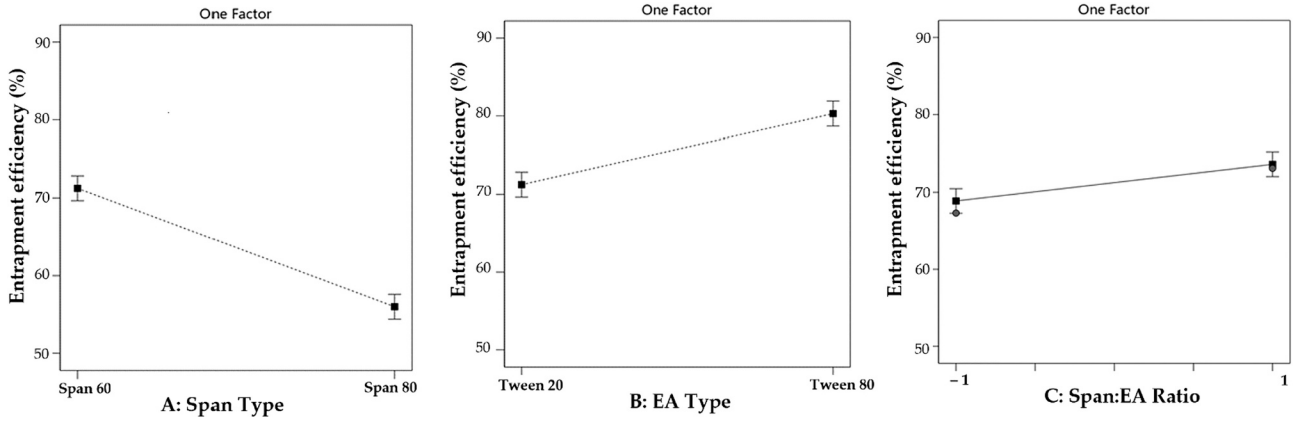

Fig. 2. The impact of various independent variables; Type of Span (A), type of EA (B), and Span:EA ratio (C) on entrapment efficiency (%).

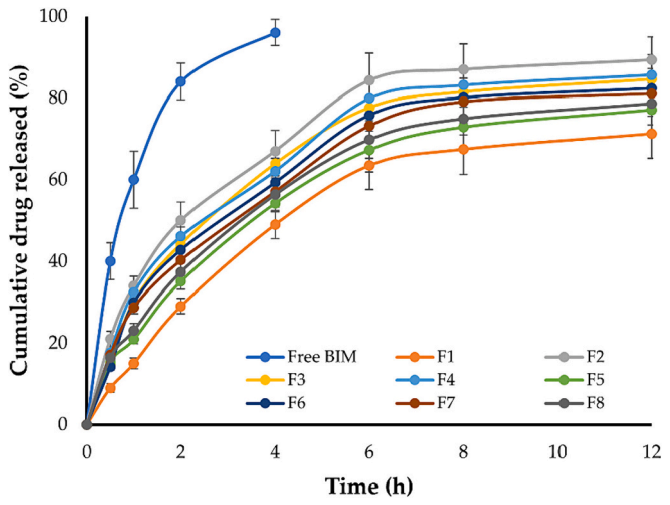

Fig. 3. *In vitro* release profile of various BIM-SLs formulations.

represented in Fig. 4. ANOVA analysis revealed that all formulation variables exerted significant effects on Q_{12h}. With respect to the type of non-ionic surfactant (A), Span 80-based BIM-SLs showed considerably higher Q_{12h} compared to Span 60 ($p < 0.001$). Such variation in drug release from various spanlastic formulation could be attributed to the differences in phase transition temperatures (T_c) among both Span 60 and Span 80. Span 60 has a T_c of 53 °C, which is comparatively higher than that of Span 80 ($T_c = -12$ °C). The higher T_c of Span 60 would favor the formation of spanlastic vesicles with more rigid bilayer membranes, compared to Span80-based vesicles.

Similarly, the type of EA (B) exerted a pronounced effect on BIM release from various spanlastic formulation. At fixed Span:EA ratio and using the same type of Span, spanlastic vesicles prepared with Tween 20, as an EA, showed a higher Q_{12h} values compared to those prepared with Tween 80. Despite having the same hydrophilic head, Tween 20 has a shorter alkyl chain length (C = 12), compared to Tween 80 (C = 18), which would bestow spanlastic bilayer membrane with more fluidity, and thereby, facilitate BIM release (Devaraj et al., 2002). These findings are in agreement with a previous report emphasizing the substantial impact of EA type (Tween 20, Tween 60 and Tween 80) on the *in vitro* release of levofloxacin from spanlastic vesicles (Agha et al., 2023).

Finally, the ratio of Span:EA (C) exerted a pronounced negative impact on Q_{12h} of the formulated BIM-SLs ($p < 0.001$). BIM-SLs prepared at Span:EA ratio of 9:1 showed considerably lower Q_{12h} compared those prepared at Span:EA ratio of 8:2. Increasing EA amount was reported to increase spanlastic bilayer membrane fluidity, and thereby, would promote higher drug release. Similar results were reported by Elsaied et al. (Elsaied et al., 2023) who highlighted the positive impact of increasing EA concentration on the *in vitro* release of the antidiabetic drug, glimepiride, from spanlastic vesicles.

3.1.4. Selection of the Optimized BIM-SLs formula

A full factorial design was adopted to analyze all tested responses of fabricated BIM-SLs formulations and select an optimized formula. A numerical optimization approach was conducted to obtain an optimized formula that complies with the required response (Table 1). F1 which was fabricated with Span 60, Tween 80 at Span:Tween ratio of 9:1, fulfilled the required criteria with a desirability of 0.949. The predicted values of F1 were 367.5 nm, 82.67% and 72.85% for R_1, R_2 and R_3, respectively, which were close to the actual values for vesicle size, % EE and Q_{12h} (364.2 ± 15.8 nm, 83.1 ± 2.1% and 71.3 ± 5.3%).

3.2. Characterization of optimized BIM-loaded Spanlastic vesicles (BIM-SLs)

3.2.1. Particle size and Zeta potential analysis

Vesicle size is considered a key determinant of skin retention/permeation behavior of drug-loaded nanovesicles. Generally, nanovesicles with particle sizes >600 nm exhibit no skin deposition (Li et al., 2022). On the other hand, nanovesicles with particle sizes <200 nm, favors transdermal drug transport (Chen et al., 2019). Importantly, nanovesicles with particle size in the range of 300–400 nm would favor the dermal delivery of their payload to the deeper skin layer, especially when they are flexible (Guillot et al., 2023). Herein, the particle size of optimized BIM-SLs (F1) was 364.2 ± 15.8 nm (Fig. 5A) with a polydispersity index of 0.289, suggesting homogenous size distribution of the formulated spanlastic vesicles.

Zeta potential is considered an important criterion to indicate the physical stability of nano-spanlastic dispersions. A zeta potential value above +20 mV or below −20 mV is considered a suitable value for vesicles stability, since high surface charge on the vesicle would ensure repulsion between the vesicles, making them stable without agglomeration (Al Hagbani et al., 2022). Herein, the optimized BIM-SLs vesicles (F1) showed a zeta potential value of −19.9 ± 2.1 mV (Fig. 5B), suggesting excellent stability of the formulated spanlastic vesicles.

3.2.2. Differential scanning calorimetric analysis

Fig. 6 depicts the DSC thermograms of BIM, Span 60, Tween 80, and optimized BIM-SLs formula (F1). As shown in Fig. 6, pure BIM displayed an endothermic peak at 72.3 °C that coincides with its melting point (Wadetwar et al., 2020). Span 60 thermogram exhibited an endothermic peak at 54.7 °C, while Tween 80 exhibited no characteristic peak (Fig. 6). Importantly, the endothermic peak of BIM were completely disappeared in the thermogram of optimized BIM-SLs formula (F1),

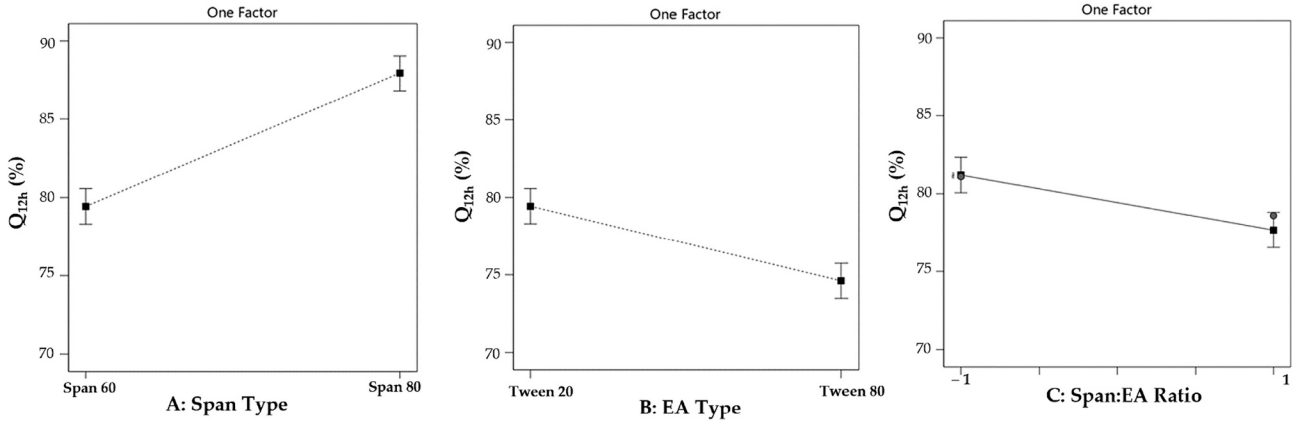

Fig. 4. The impact of various independent variables; Type of Span (A), type of EA (B), and Span:EA ratio (C) on percentage drug released at 12 h (Q_{12h}).

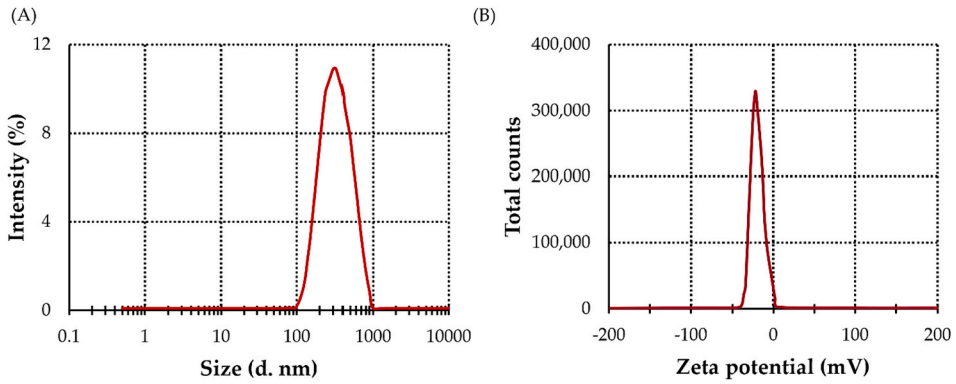

Fig. 5. (A)Vesicle size and (B) Zeta potential of optimized BIM-SLs formula (F1).

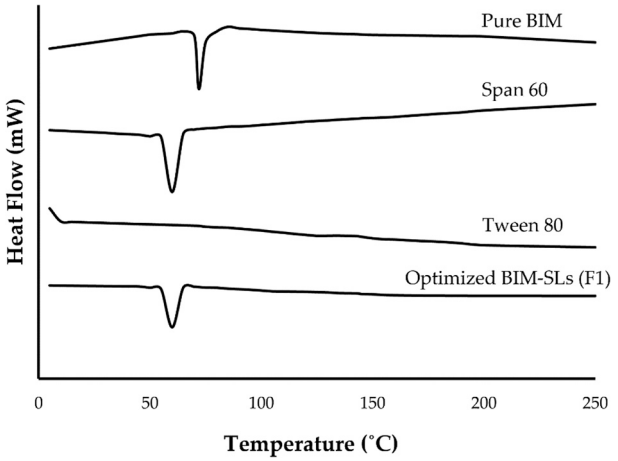

Fig. 6. DSC thermograms of pure BIM, Span 60, Tween 80 and optimized BIM-SLs formula.

suggesting a complete entrapment of BIM and its transformation from the crystalline form to the amorphous form (Zafar et al., 2022). Collectively, DSC analysis nullified any incompatibility between BIM and formulation components.

3.2.3. Elasticity of optimized BIM-SLs formula (F1)

The degree of elasticity of spanlastic vesicles is an important parameter as it reflects the ability of elastic vesicles to cross biological membranes. The elasticity of spanlastics was measured in terms of the deformability index (DI) using the extrusion technique. DI indicates vesicles' ability to squeeze through skin pores that are smaller in size than their own diameter without rupture. The optimized BIM-SLs formula (F1) showed a DI of 10.48 ± 1.6, suggesting high deformability and good elasticity (Elhabak et al., 2021). EA in spanlastics destabilizes the lipid bilayer, enhancing its elasticity (Hussain et al., 2017). In addition, the unsaturated non-bulky alkyl chains of Tween 80 make it more deformable and elastic, and thereby, would augment their permeability through biological membranes.

3.3. Stability of the Optimized BIM-SLs formula (F1)

The influence of storage for 90 days at 4 °C on the stability of the optimized BIM-SLs formula (F1) was demonstrated in Table 5. It was evident that optimized BIM-SLs retained good physical stability as manifested by the absence of significant changes ($p > 0.05$) in the vesicle size, surface charge and percentage drug entrapped of the stored spanlastics compared to fresh formula.

Table 5
Stability o optimized BIM-SLs formula (F1).

Parameter	Day 0	Day 30	Day 90
Vesicle size (nm)	364.2 ± 15.8	373.4 ± 13.7	389.3 ± 21.9
Zeta potential (mV)	– 19.9 ± 2.1	– 19.2 ± 1.8	– 17.3 ± 1.9
Entrapment efficiency (%)	83.1 ± 2.1	82.4 ± 2.0	81.3 ± 2.9

3.4. Formulation and characterization of LSG

The optimized BIM-SLs formula was incorporated into gel formulation to enhance the adherence of applied nanovesicles to the skin site, prolong residence time, and thereby, boost drug permeation through skin surface. Prescreening studies were performed to determine the most appropriate gelling agent for formulating BIM-loaded spanlastic gel (BIM-SLG). A variety of gelling agents, such as Carbopol 934, methylcellulose and hydroxypropyl methylcellulose (HPMC) were adopted for the fabrication of BIM-SLG and were investigated for their physicochemical characteristics. Among them, hydrogels prepared with HPMC had better physicochemical characteristics in terms of homogeneity, consistency, and spreadability than hydrogels prepared with either Carbopol 934 or methylcellulose. Accordingly, HPMC-based hydrogel loaded with BIM-SLs vesicles were selected for further investigations.

The pH of BIM-SLG was 4.94 ± 0.2, which is compatible with scalp hair. The drug content was 98.1 ± 0.6%, indicating good drug loading within hydrogel. The gel sample had a spreadability value of 5.72 ± 0.8 cm, suggesting that the formulation would be easily spreadable (Nurman et al., 2019). Finally, BIM-SLG showed a relatively low viscosity of 3938.6 ± 199 Cps, which is considered acceptable for topical application (Shiehzadeh et al., 2023).

3.5. In vitro release of BIM from BIM-SLG

Fig. 7 depicts BIM *in vitro* release profile from BIM-SLG compared to either pure BIM-loaded HPMC hydrogel or optimized BIM-SLs formula (F1). It was evident that BIM-SLG extended BIM release compared to both F1 and BIM-loaded hydrogel. Such sustained drug release might be ascribed to the dual action of incorporating a vesicular system, spanlastics, within the gel.

3.6. Ex vivo skin permeability study

To scrutinize the influence of drug carrier on drug diffusion through the skin and deposition in the hair follicle, an *ex vivo* permeation study of BIM-loaded spanlastic gel (BIM-SLG) was conducted and compared to that of optimized BIM-SLs formula (F1) and naive BIM gel. As depicted in Fig. 8, encapsulation of BIM within spanlastic nanovesicles remarkably hindered the effective permeation of BIM through abdominal rat skin compared to naive BIM gel. The cumulative amounts of BIM

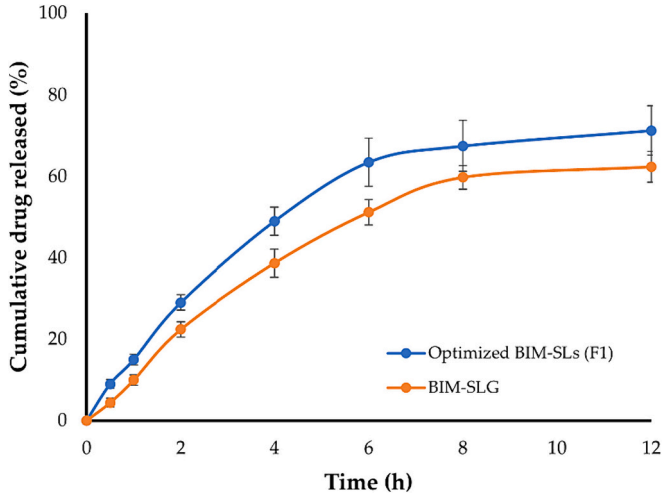

Fig. 7. Comparison between the *in vitro* release profile of BIM from optimized spanlastic formula and Spanlastic loaded gel.

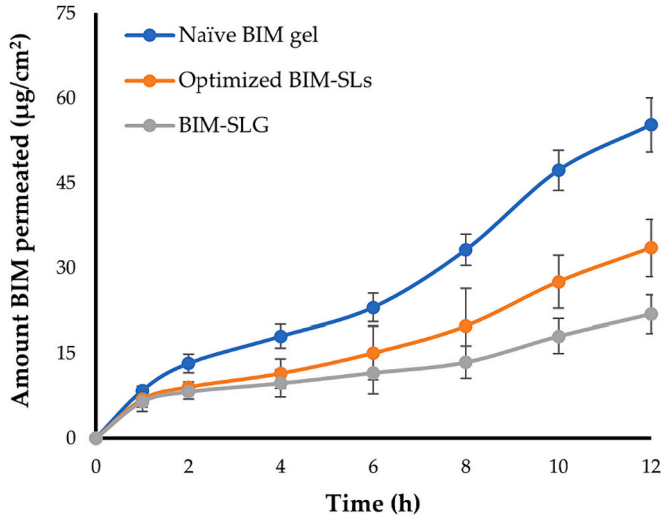

Fig. 8. *Ex vivo* permeation profile of BIM from various BIM-loaded formulations.

permeated through rat skin at 12 h (Q_{12h}) were 55.25 ± 4.76, 33.51 ± 5.07, and 21.84 ± 3.44 µg/cm^2, for naïve BIM gel, BIM-SLs (F1), and BIM-SLG, respectively. Instead, spanlastic vesicles promoted BIM accumulation within skin layers as demonstrated by the higher skin deposition of BIM from both optimized BIM-SLs formula (F1) and BIM-SLG, compared to naïve BIM gel. The cumulative amounts of BIM deposited into rat skin at 12 h (Dep_{12h}) were 123.31 ± 15.2, 284.72 ± 21.0, and 350.57 ± 32.3 µg/cm^2, for naïve BIM gel, BIM-SLs (F1), and BIM-SLG, respectively (Table 6). The calculated local accumulation efficiency index (LAEI) value of both BIM-SLs (F1) and BIM-SLG was ~3- and 5-folds higher than that of naïve BIM gel, respectively. This superior cutaneous accumulation of spanlastic vesicles might be accredited to their relatively large vesicle size (>300 nm), which would favor spanlastic retention within skin layers rather than being permeated through the skin, as noticed with naïve BIM gel. It is worth noting that incorporating spanlastic vesicles into HPMC gel slowed down BIM release from the gel network compared to spanlastic dispersion, resulting in a lower transdermal flux of BIM compared to BIM-SLs (F1) (Table 6). Collectively, it was evident that entrapment of BIM within spanlastic vesicles would be a viable mean to enhance BIM cutaneous retention while minimizing its skin permeation, and thereby, nullifying the possibility of eliciting systemic side effects.

Table 6
Permeation parameters of various BIM formulations.

Permeation parameter	Naïve BIM gel	Optimized BIM-SLs	BIM-SLG
Q_{12h} (µg/cm^2)	55.25 ± 4.76	33.51 ± 5.07	21.84 ± 3.44
J_{ss} (µg/h.cm^2)	4.61 ± 0.40	2.79 ± 0.42	1.49 ± 0.29
Dep_{12h} (µg/cm^2)	173.10 ± 15.19	284.72 ± 21.03	314.27 ± 13.96
LAEI	3.13 ± 0.32	8.49 ± 0.41	14.39 ± 0.94

3.7. *In vivo dermato-kinetic study*

The *in vivo* dermato-kinetic study offers a realistic mean for assessing drug deposition within skin layers following topical treatment. As illustrated in Fig. 9, BIM-loaded spanlastic gel exerted superior drug retention in the skin; the maximum drug concentration in skin layers (C_{max}) of BIM-SLG (158.57 ± 14.49 µg/mL) was significantly higher ($p < 0.05$) than that of naïve BIM gel (C_{max} 67.10 ± 7.93 µg/mL). Most importantly, the $AUC_{0\text{-}12h}$ of BIM-SLG was twice as high as naïve BIM gel. The $AUC_{0\text{-}12h}$ values of BIM-SLG and naïve BIM gel were 888.05 ± 72.31 µg/mL.h, and 382.86 ± 41.12 µg/mL.h, respectively. These results consolidate with the *ex-vivo* permeation findings, indicating that topically applied spanlastic vesicles could partition across the subcutaneous layer under the influence of the transcutaneous hydration gradient, forming depots from which BIM can be released (Peira et al., 2007). Our findings are in alignment with those of Aldawsari et al. (Aldawsari et al., 2023) who inferred the superior efficacy of niosomal vesicles to permit efficient cutaneous deposition of cetirizine, compared to naïve cetirizine gel, for the management of alopecia.

3.8. *In vivo hair regrowth evaluation*

An androgenetic alopecia mouse model was adopted to assess hair regrowth status, in terms of hair weight and hair follicle length, following treatment with different BIM formulations. As depicted in Fig. 10A, the vehicle-treated (BIM-free blank spanlastic) group had reduced hair weight than the control group (normal), indicating that androgenic alopecia caused delayed hair regeneration. Hair weight in normal control group was 4.61 ± 0.64 mg, which was greater than that of blank spanlastic-treated control (2.92 ± 0.52 mg). In addition, the hair weight of BIM-SLG treated group (51.67 ± 3.38 mg) was comparatively ($p < 0.05$) higher than that of control (vehicle; 2.92 ± 0.52 mg) and naïve BIM gel treated groups (15.28 ± 3.37 mg). Of interest, at 14 days post treatment, hair regrowth efficiency of BIM-SLG was superior to that of minoxidil-treated group; hair weight of BIM-SLG-treated group

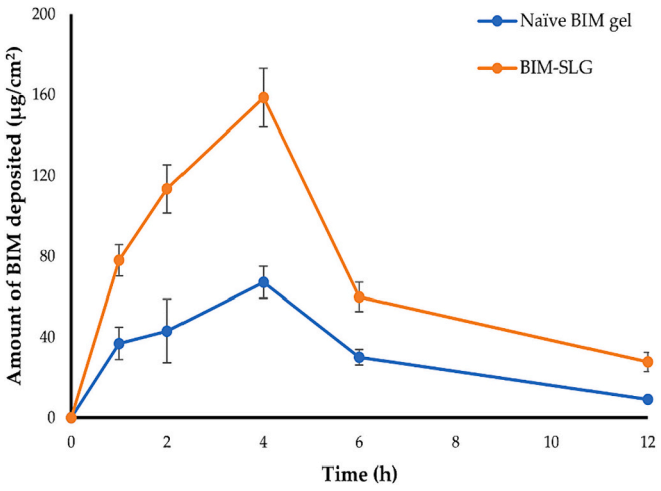

Fig. 9. *In vivo* skin deposition profile of BIM from naive BIM gel and BI-SLG.

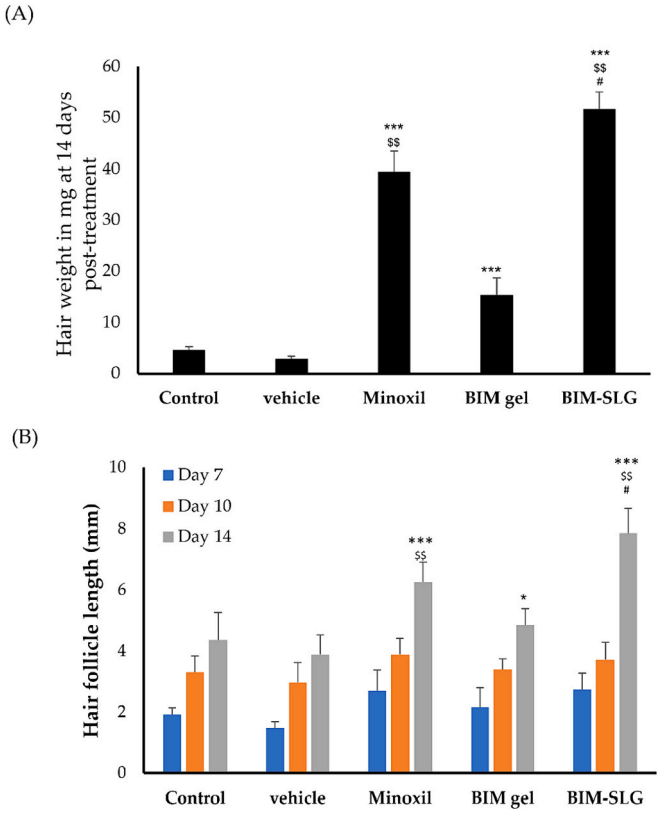

Fig. 10. (A) Hair weights for each group at 14 days post-treatment. (B) Length of hair follicles at 7-, 10-, and 14-days post-treatment. $^{*}p < 0.05$ and $^{***}p < 0.001$ *vs* vehicle control; $^{\$\$}p < 0.01$ *vs* naïve BIM gel; $^{\#}p < 0.05$ *vs* minoxidil-treated mice.

was 1.3-fold as high as commercial minoxidil-treated group. These results demonstrate the efficacy of BIM-SLG to promote the formation of dense hair follicles.

Additionally, the length of hair follicles of newly grown hairs was measured at different time intervals post treatment with various formulations. As illustrated in Fig. 10B, regardless treatment duration, the length of hair follicles in mice treated with either BIM formulations or commercial minoxidil formulation were higher than those in the control (normal) and control (vehicle) groups. At seven days post-treatment, the length of hair follicles of minoxidil-, naïve BIM gel-, and BIM-SLG-treated groups was 2.7 ± 0.68 mm, 2.15 ± 0.65 mm, and 2.74 ± 0.54 mm, respectively, which was remarkably longer than that of either control (normal) or control (vehicle) groups (1.92 ± 0.22 mm and 1.48 ± 0.20 mm, respectively). Nevertheless, up to ten days post-treatment, hair follicles length among naïve BIM gel and commercial minoxidil solution was comparable to that of BIM-SLG-treated group. Intriguingly, at 14 days post treatment, mice treated with BIM-SLG had hair follicles of 7.86 ± 0.82 mm in length, which was significantly longer than those from mice treated with naïve BIM gel (4.85 ± 0.54 mm), and commercial minoxidil topical solution (6.26 ± 0.82 mm). Collectively, hair growth evaluation results clearly highlight the improved hair regrowth efficacy of BIM-SLG, which might be accredited to the propensity of spanlastic vesicles to permeate through different skin layers and their efficiency to deliver adequate quantities of their payload (BIM) to deep dermal layers, resulting in maximal activation of dermal papilla cells and keratinocytes, promoting superior hair follicles growth compared to naive BIM gel. Nevertheless, further research is needed to optimize treatment concentrations *in vivo* and to elucidate the underlying mechanisms of the activation of hair growth.

4. Conclusions

This study revealed the repurposing of topical prostaglandin analog, bimatoprost (BIM), for the management of androgenic alopecia, as well as tailoring of spanlastic-based nanogel laden with BIM to enhance cutaneous delivery. BIM-loaded spanlastic vesicles (BIM-SLs) were fabricated by the ethanol injection technique using Span 60 as the main vesicle component and Tween 80 as an edge activator. The fabricated spanlastic vesicles were optimized by 2^3 full factorial Design. The optimized formula exhibited high drug entrapment efficiency, appropriate zeta potential, and a vesicle size of 364.2 ± 15.8 nm, which favored their cutaneous accumulation. In addition, *ex-vivo* skin deposition test clearly demonstrated that BIM-loaded spanlastic gel (BIM-SLG) facilitated superior drug deposition into skin than naïve BIM gel. Most notably, *in vivo* experiments confirmed that BIM-SLG had preferential cutaneous accumulation than naive BIM gel, as evidenced by a two-fold rise in $AUC_{0\text{-}12h}$. Furthermore, BIM-SLG surpasses both naïve BIM gel and commercial minoxidil formulation in activating hair growth in an androgenetic alopecia mouse model. To summarize, spanlastic vesicles might be a potential platform that enhance and sustain the cutaneous delivery of the topical prostaglandin analog, BIM, for the management of alopecia.

Institutional review board statement

The animal study protocol was approved by the Ethical Committee, Prince Sattam Bin Abdulaziz University, Al-Kharj, KSA (approval number: 048/2022).

CRediT authorship contribution statement

Bjad K. Almutairy: Methodology, Investigation, Conceptualization. **El-Sayed Khafagy:** Data curation, Conceptualization. **Mohammed F. Aldawsari:** Formal analysis, Data curation. **Abdullah Alshetaili:** Software, Formal analysis. **Hadil Faris Alotaibi:** Project administration, Funding acquisition, Formal analysis. **Amr Selim Abu Lila:** Writing – review & editing, Writing – original draft.

Declaration of competing interest

The authors declare no conflicts of interest.

Data availability

Data will be made available on request.

Acknowledgments

This research is supported *via* funding from Prince Sattam Bin Abdulaziz University project number (PSAU/2024/R/1445). The authors also extend their appreciation to the Princess Nourah bint Abdulrahman University, Riyadh, Saudi Arabia for supporting this work under the researcher supporting project number (PNURSP2024R205).

References

Abu-Huwaij, R., Alkarawi, A., Salman, D., Alkarawi, F., 2023. Exploring the use of niosomes in cosmetics for efficient dermal drug delivery. Pharm. Dev. Technol. 28, 708–718.
Adil, A., Godwin, M., 2017. The effectiveness of treatments for androgenetic alopecia: a systematic review and meta-analysis. J. Am. Acad. Dermatol. 77 (136–141), e135.
Agha, O.A., Girgis, G.N.S., El-Sokkary, M.M.A., Soliman, O.A.E., 2023. Spanlastic-laden in situ gel as a promising approach for ocular delivery of Levofloxacin: In-vitro characterization, microbiological assessment, corneal permeability and in-vivo study. Int. J. Pharm. X 6, 100201.
Akbari, V., Abedi, D., Pardakhty, A., Sadeghi-Aliabadi, H., 2015. Release Studies on Ciprofloxacin Loaded Non-ionic Surfactant Vesicles. Avicenna J. Med. Biotechnol. 7, 69–75.

Al Hagbani, T., Rizvi, S.M.D., Hussain, T., Mehmood, K., Rafi, Z., Moin, A., Abu Lila, A.S., Alshammari, F., Khafagy, E.S., Rahamathulla, M., Abdallah, M.H., 2022. Cefotaxime Mediated Synthesis of Gold Nanoparticles: Characterization and Antibacterial activity. Polymers (Basel) 14, 771.
Al Saqr, A., Wani, S.U.D., Gangadharappa, H.V., Aldawsari, M.F., Khafagy, E.S., Lila, A.S. A., 2021. Enhanced Cytotoxic activity of Docetaxel-Loaded Silk Fibroin Nanoparticles against Breast Cancer Cells. Polymers (Basel) 13, 1416.
Albash, R., Fahmy, A.M., Hamed, M.I.A., Darwish, K.M., El-Dahmy, R.M., 2021. Spironolactone hyaluronic acid enriched cerosomes (HAECs) for topical management of hirsutism: in silico studies, statistical optimization, ex vivo, and in vivo studies. Drug Deliv. 28, 2289–2300.
Albash, R., El-Dahmy, R.M., Hamed, M.I.A., Darwish, K.M., Alahdal, A.M., Kassem, A.B., Fahmy, A.M., 2022. Repurposing levocetirizine hydrochloride loaded into cationic ceramide/phospholipid composite (CCPCs) for management of alopecia: central composite design optimization, in- silico and in-vivo studies. Drug Deliv. 29, 2784–2795.
Aldawsari, M.F., Khafagy, E.S., Moglad, E.H., Selim Abu Lila, A., 2023. Formulation optimization, in vitro and in vivo evaluation of niosomal nanocarriers for enhanced topical delivery of cetirizine. Saudi Pharm J 31, 101734.
Al-mahallawi, A.M., Khowessah, O.M., Shoukri, R.A., 2017. Enhanced non invasive trans-tympanic delivery of ciprofloxacin through encapsulation into nano-spanlastic vesicles: Fabrication, in-vitro characterization, and comparative ex-vivo permeation studies. Int. J. Pharm. 522, 157–164.
Almutairy, B.K., Khafagy, E.S., Abu Lila, A.S., 2023. Development of Carvedilol Nanoformulation-Loaded Poloxamer-based in Situ Gel for the Management of Glaucoma. Gels 9, 952.
Ansari, M.D., Saifi, Z., Pandit, J., Khan, I., Solanki, P., Sultana, Y., Aqil, M., 2022. Spanlastics a Novel Nanovesicular carrier: its potential Application and Emerging Trends in Therapeutic delivery. AAPS PharmSciTech 23, 112.
Badria, F., Mazyed, E., 2020. Formulation of Nanospanlastics as a Promising Approach for improving the Topical delivery of a Natural Leukotriene Inhibitor (3-Acetyl-11-Keto-β-Boswellic Acid): Statistical Optimization, in vitro Characterization, and ex vivo Permeation Study. Drug Des. Devel. Ther. 14, 3697–3721.
Barrón-Hernández, Y.L., Tosti, A., 2017. Bimatoprost for the treatment of eyelash, eyebrow and scalp alopecia. Expert Opin. Investig. Drugs 26, 515–522.
Basha, M., Abd El-Alim, S.H., Shamma, R.N., Awad, G.E., 2013. Design and optimization of surfactant-based nanovesicles for ocular delivery of Clotrimazole. J. Liposome Res. 23, 203–210.
Chen, S., Hanning, S., Falconer, J., Locke, M., Wen, J., 2019. Recent advances in non-ionic surfactant vesicles (niosomes): Fabrication, characterization, pharmaceutical and cosmetic applications. Eur. J. Pharm. Biopharm. 144, 18–39.
Chen, X., Xiang, H., Yang, M., 2022. Topical cetirizine for treating androgenetic alopecia: a systematic review. J. Cosmet. Dermatol. 21, 5519–5526.
Cohen, J.L., 2010. Enhancing the growth of natural eyelashes: the mechanism of bimatoprost-induced eyelash growth. Dermatologic Surg. 36, 1361–1371.
Devaraj, G.N., Parakh, S.R., Devraj, R., Apte, S.S., Rao, B.R., Rambhau, D., 2002. Release studies on niosomes containing fatty alcohols as bilayer stabilizers instead of cholesterol. J. Colloid Interface Sci. 251, 360–365.
Duangjit, S., Opanasopit, P., Rojanarata, T., Ngawhirunpat, T., 2011. Characterization and in Vitro Skin Permeation of Meloxicam-Loaded Liposomes versus Transfersomes. J. Drug Deliv. 2011, 418316.
Elhabak, M., Ibrahim, S., Abouelatta, S.M., 2021. Topical delivery of l-ascorbic acid spanlastics for stability enhancement and treatment of UVB induced damaged skin. Drug Deliv. 28, 445–453.
ElMeshad, A.N., Mohsen, A.M., 2016. Enhanced corneal permeation and antimycotic activity of itraconazole against Candida albicans via a novel nanosystem vesicle. Drug Deliv. 23, 2115–2123.
Elsaied, E.H., Dawaba, H.M., Ibrahim, E.S.A., Afouna, M.I., 2023. Spanlastics gel-a novel drug carrier for transdermal delivery of glimepiride. J. Liposome Res. 33, 102–114.
Farghaly, D.A., Aboelwafa, A.A., Hamza, M.Y., Mohamed, M.I., 2017. Topical delivery of Fenoprofen Calcium via Elastic Nano-vesicular Spanlastics: Optimization using Experimental Design and in Vivo Evaluation. AAPS PharmSciTech 18, 2898–2909.
Fu, D., Huang, J., Li, K., Chen, Y., He, Y., Sun, Y., Guo, Y., Du, L., Qu, Q., Miao, Y., Hu, Z., 2021. Dihydrotestosterone-induced hair regrowth inhibition by activating androgen receptor in C57BL6 mice simulates androgenetic alopecia. Biomed. Pharmacother. 137, 111247.
Gokce, N., Basgoz, N., Kenanoglu, S., Akalin, H., Ozkul, Y., Ergoren, M.C., Beccari, T., Bertelli, M., Dundar, M., 2022. An overview of the genetic aspects of hair loss and its connection with nutrition. J. Prev. Med. Hyg. 63, E228–E238.
Guillot, A.J., Martínez-Navarrete, M., Garrigues, T.M., Melero, A., 2023. Skin drug delivery using lipid vesicles: a starting guideline for their development. J. Control. Release 355, 624–654.
Guinedi, A.S., Mortada, N.D., Mansour, S., Hathout, R.M., 2005. Preparation and evaluation of reverse-phase evaporation and multilamellar niosomes as ophthalmic carriers of acetazolamide. Int. J. Pharm. 306, 71–82.
Heilmann, S., Nyholt, D.R., Brockschmidt, F.F., Hillmer, A.M., Herold, C., Becker, T., Martin, N.G., Nöthen, M.M., 2013. No genetic support for a contribution of prostaglandins to the aetiology of androgenetic alopecia. Br. J. Dermatol. 169, 222–224.
Hussain, A., Singh, S., Sharma, D., Webster, T.J., Shafaat, K., Faruk, A., 2017. Elastic liposomes as novel carriers: recent advances in drug delivery. Int. J. Nanomedicine 12, 5087–5108.
Jiang, S., Hao, Z., Qi, W., Wang, Z., Zhou, M., Guo, N., 2023. The efficacy of topical prostaglandin analogs for hair loss: a systematic review and meta-analysis. Front. Med. (Lausanne) 10, 1130623.
Law, S.K., 2010. Bimatoprost in the treatment of eyelash hypotrichosis. Clin. Ophthalmol. 4, 349–358.
Li, D., Martini, N., Wu, Z., Chen, S., Falconer, J.R., Locke, M., Zhang, Z., Wen, J., 2022. Niosomal Nanocarriers for Enhanced Dermal delivery of Epigallocatechin Gallate for Protection against Oxidative stress of the Skin. Pharmaceutics 14, 726.
Mazyed, E.A., Helal, D.A., Elkhoudary, M.M., Abd Elhameed, A.G., Yasser, M., 2021. Formulation and Optimization of Nanospanlastics for improving the Bioavailability of Green Tea Epigallocatechin Gallate. Pharmaceuticals (Basel) 14, 68.
Moawad, F.A., Ali, A.A., Salem, H.F., 2017. Nanotransfersomes-loaded thermosensitive in situ gel as a rectal delivery system of tizanidine HCl: preparation, in vitro and in vivo performance. Drug Deliv. 24, 252–260.
Nurman, S., Yulia, R., Irmayanti, Noor E., Candra Sunarti, T., 2019. The Optimization of Gel Preparations using the active Compounds of Arabica Coffee Ground Nanoparticles. Sci. Pharm. 87, 32.
Orasan, M.S., Roman, I.I., Coneac, A., Muresan, A., Orasan, R.I., 2016. Hair loss and regeneration performed on animal models. Clujul Med. 89, 327–334.
Peira, E., Trotta, M., Carlotti, M.E., Gallarate, M., Chirio, D., 2007. Elastic positively-charged liposomes for topical administration of acyclovir. J. Drug Deliv. Sci. Technol. 17, 321–324.
Pierre, M.B.R., dos Santos Miranda Costa, I., 2011. Liposomal systems as drug delivery vehicles for dermal and transdermal applications. Arch. Dermatol. Res. 303, 607–621.
Qi, J., Garza, L.A., 2014. An Overview of Alopecias. Cold Spring Harb Perspect Med, p. 4.
Ruckmani, K., Sankar, V., 2010. Formulation and optimization of Zidovudine niosomes. AAPS PharmSciTech 11, 1119–1127.
Sallam, M.A., Prakash, S., Kumbhojkar, N., Shields Iv, C.W., Mitragotri, S., 2021a. Formulation-based approaches for dermal delivery of vaccines and therapeutic nucleic acids: recent advances and future perspectives. Bioeng. & Translat. Med. 6, e10215.
Sallam, N.M., Sanad, R.A.B., Ahmed, M.M., Khafagy, E.L.S., Ghorab, M., Gad, S., 2021b. Impact of the mucoadhesive lyophilized wafer loaded with novel carvedilol nano-spanlastics on biochemical markers in the heart of spontaneously hypertensive rat models. Drug Deliv. Transl. Res. 11, 1009–1036.
Satyanarayana, S.D., Abu Lila, A.S., Moin, A., Moglad, E.H., Khafagy, E.S., Alotaibi, H.F., Obaidullah, A.J., Charyulu, R.N., 2023. Ocular delivery of Bimatoprost-Loaded Solid Lipid Nanoparticles for Effective Management of Glaucoma. Pharmaceuticals (Basel) 16, 1001.
Schreier, H., Bouwstra, J., 1994. Liposomes and niosomes as topical drug carriers: dermal and transdermal drug delivery. J. Control. Release 30, 1–15.
Shiehzadeh, F., Mohebi, D., Chavoshian, O., Daneshmand, S., 2023. Formulation, Characterization, and Optimization of a Topical Gel Containing Tranexamic Acid to Prevent Superficial Bleeding: In Vivo and In Vitro Evaluations. Turk. J. Pharm. Sci. 20, 261–269.
Subedi, L., Pandey, P., Shim, J.H., Kim, K.T., Cho, S.S., Koo, K.T., Kim, B.J., Park, J.W., 2022. Preparation of topical bimatoprost with enhanced skin infiltration and in vivo hair regrowth efficacy in androgenic alopecia. Drug Deliv. 29, 328–341.
Suchonwanit, P., Thammarucha, S., Leerunyakul, K., 2019. Minoxidil and its use in hair disorders: a review. Drug Des. Devel. Ther. 13, 2777–2786.
Tabri, F., Anwar, A.I., Adriani, A., DwiAryaningrum, 2018. The Efectiveness of 0.03% Bimatoprost solution Vs Minoxidil 5% in Androgenic Alopecia. Indian J. Publ. Health Res. Develop. 9, 1444.
Wadetwar, R.N., Agrawal, A.R., Kanojiya, P.S., 2020. In situ gel containing Bimatoprost solid lipid nanoparticles for ocular delivery: In-vitro and ex-vivo evaluation. J. Drug Deliv. Sci. Technol. 56, 101575.
Yusuf, M., Sharma, V., Pathak, K., 2014. Nanovesicles for transdermal delivery of felodipine: Development, characterization, and pharmacokinetics. Int. J. Pharm. Investig. 4, 119–130.
Zafar, A., Alsaidan, O.A., Imam, S.S., Yasir, M., Alharbi, K.S., Khalid, M., 2022. Formulation and Evaluation of Moxifloxacin Loaded Bilosomes In-Situ Gel: Optimization to Antibacterial Evaluation. Gels 8, 418.
Zezula, M., Ruszczak, M., Maruszak, W., Zagrodzka, J., Chodynski, M., Dams, I., 2019. Development and validation of the stability indicating RP-UHPLC method for the determination of the chemical purity and assay of bimatoprost. J. Pharm. Biomed. Anal. 174, 348–359.
Zhang, T., Cao, S., Yuan, H., Park, S., 2021. Alleviation of Androgenetic Alopecia with Aqueous Paeonia lactiflora and Poria cocos Extract Intake through Suppressing the Steroid Hormone and Inflammatory Pathway. Pharmaceuticals (Basel) 14, 1128.